Comm. Korean Math. Soc. 10 (1995), No. 3, pp. 767-781

REFLECTIONS OF SHOCKS IN NONEQUILIBRIUM FLOW OF AIR

TAEHOON PARK

ABSTRACT. In this paper we present computation of a reflected shock in the hypersonic flow of air with chemical reactions. We consider two dimensional steady inviscid hypersonic flow of air around bodies including chemical reaction effects. At a high Mach number, a strong shock is formed in front of the body when a wedge is placed against the flow. In front of the shock, the flow is uniform and the temperature is low. Behind the shock, temperature and pressure increase greatly and the flow is in nonequilibrium state. If the shock hits a wall, then a reflected shock is formed in the nonequlibrium flow region. Behind this reflected shock, the temperature and pressure are very high. We carry out the computation of the reflected shock and the flow behind it. The jump conditions at the reflected shock are presented. A technique combining smooth transforms of domain and implicit difference methods is used to overcome numerical difficulties associated with the lack of resolution behind the shock and near the body.

1. Introduction

The problem we consider is the computation of reflected shock in nonequilibrium hypersonic inviscid flow. As is well known, there are two types of numerical methods to deal with shock problems, one is the shock-capturing methods and the other is the shock-fitting methods. Among the second type of methods, there is a technique called the Singularity-Separating Method [7], by which the interaction of discontinuities for steady supersonic flow could be computed accurately. We use similar method to compute a reflected shock for steady hypersonic inviscid flow with chemical reactions considered. Since the reflected shock

Received March 14, 1995. Revised June 3, 1995.
1991 AMS Subject Classification: 76-08, 76M20.
Key words: Nonequilibrium air, Finite difference method, Shock reflection.
This work was supported by TGRC-KOSEF.

occurs in the chemical reaction region behind the main shock, the temperature and pressure are much higher behind this shock than behind the main shock. This causes very strong chemical reactions which make the computation difficult. We use implicit scheme to overcome the stiffness associated with this kind of phenomena.

For numerical experiment, we generated a shock by placing a wedge against the free stream. At a high Mach number, a strong shock is formed in front of the body. The flow is uniform and the temperature is low in front of the shock. We have reported the computation of this shock for a long distance in [3] enhancing the result of [2]. If we place a wall against the shock, the shock is reflected. The reflected shock is formed behind the original shock. Since the reflected shock is formed in the nonequilibrium region, the jump conditions are different from those at the main shock. We derive the jump conditions at the reflected shock from the Rankine-Hugoniot conditions. With the successful computation of the main shock and the flow properties accurately [3], we could compute the reflected shock. The computation is difficult near the reflection point because the flow properties change greatly in a short distance. Once the computation is successful for a short distance from the reflection point, it is relatively easy to continue the computation for longer distance as the computation of the main shock in [3]. The numerical results are reported in Section 4. We reported the flow properties for a short distance from the reflection point.

2. System of equations

Following the presentation given in [5], we consider the continuity, momentum and energy equations:

$$
\begin{aligned}
&\mathbf{V}\cdot\nabla\rho+\rho\nabla\cdot\mathbf{V}=0,\\
&(\mathbf{V}\cdot\nabla)\mathbf{V}+\frac{\nabla p}{\rho}=0,\\
&\mathbf{V}\cdot\left(\nabla h-\frac{\nabla p}{\rho}\right)=0,
\end{aligned}
\tag{1}
$$

where $\mathbf{V}$, ρ, p and h denote the velocity vector, density, pressure and enthalpy, respectively. In our chemical model of air there are 5 species

and 18 reactions. The species are O, N, NO, O_2, N_2, which we call the first, ..., the fifth species respectively in what follows. Also the vibrational excitation of biatomic molecules is assumed half-excited so that its energy content is $RT/2$. We neglect the diffusion of the species and we write the equations of the production of the species along streamlines:

$$\mathbf{V} \cdot \nabla q_i = \omega_i, \quad i = 1, 2, 3.$$

Here, q_i denotes the concentration in unit $g - mole \cdot g^{-1}$ and the source term ω_i gives the rate of production for the i-th species.

Moreover, we have the state equation :

$$p = \rho R T \mathcal{Z}, \tag{2}$$

$$h = \frac{p}{\rho} \frac{3 + \mathcal{Z}}{\mathcal{Z}} + \sum_{i=1}^{3} h_i^0 q_i, \tag{3}$$

where the compressibility factor $\mathcal{Z}$ is

$$\mathcal{Z} = 1 + \mu \frac{q_1 + q_2}{2}$$

and h_i^0 are the formation energies of the species O, N and NO given in [5]. Finally, the mass conservation law provides the concentration q_4 and q_5 of the fourth species O_2 and the fifth species N_2, respectively:

$$q_4 = \frac{0.21}{\mu} - \frac{q_1 + q_3}{2}, \quad q_5 = \frac{0.79}{\mu} - \frac{q_2 + q_3}{2},$$

where μ is the average molecular weight of air that is $28.8 g/g - mole$. The reaction rates ω_i in unit of $g - mole \cdot g^{-1} \cdot s^{-1}$ and all the formulae and coefficients needed for calculating ω_i can be found in [5].

On the basis of the above equations, we can relate the derivatives of the pressure and density :

$$\mathbf{V} \cdot \nabla \rho = \frac{1}{a^2} \mathbf{V} \cdot \nabla p - \Psi. \tag{4}$$

Here, a defines the frozen speed of sound:

$$a^2 = \frac{\partial h/\partial \rho}{1/\rho - \partial h/\partial p}, \tag{5}$$

and the term Ψ depends on the rates of production ω_i of species:

$$\Psi = \sum_{i=1}^{3} \omega_i \frac{\partial h/\partial q_i}{\partial h/\partial \rho}. \tag{6}$$

We now describe the equations for a two dimensional computational frame $\{\xi, \eta\}$. Using equation (7), we write the Euler equations (1) in terms of $(p, h, \mathbf{V})$ as dependent variables. Then we introduce the slope of a streamline

$$\sigma = \frac{v}{u},$$

where u and v are the velocity components. The Euler and the chemical equations then become

$$\left(1 - \frac{a^2}{u^2}\right) p_z + \sigma p_r + \rho a^2 \sigma_r = \frac{a^2}{u}\Psi, \tag{7}$$

$$\sigma_z + \sigma\sigma_r + \frac{p_r - \sigma p_z}{\rho u^2} = 0, \tag{8}$$

$$h_z - \frac{p_z}{\rho} + \sigma\left(h_r - \frac{p_r}{\rho}\right) = 0, \tag{9}$$

$$(q_i)_z + \sigma(q_i)_r = \frac{\omega_i}{u}, \quad i = 1, 2, 3. \tag{10}$$

The system is completed by the integrated form of the energy equation

$$\begin{aligned} H &= h + \frac{V^2}{2} \\ &= \text{constant}, \end{aligned} \tag{11}$$

where $V = \sqrt{u^2 + v^2}$ is the speed of the flow.

The region confined by $r = b(\eta)$, $r = c(\eta)$, $\eta = \eta_0^*$ and $\eta = \eta_1^*$ is the physical domain for computation. The curve $r = b(\eta)$ is the body and

$r = c(\eta)$ is the reflected shock and $\eta = \eta_0^*$ is the point of reflection. We now introduce a computational frame (η, ξ)

$$z = \eta \quad (\eta_0^* \leq \eta \leq \eta_1^*),$$
$$r = G(\eta, \xi).$$

Here $G(\eta, \xi)$ satisfies the conditions $b(\eta) = G(\eta, 0)$ and $c(\eta) = G(\eta, 1)$ so that $\xi = 0$ at the body and $\xi = 1$ at the shock and the computational domain under the (η, ξ) coordinate system is a rectangle. The derivatives with respect to z and r in (7)-(10)can be changed into the derivatives with respect to η and ξ and we obtain the corresponding system of equations under the (η, ξ) coordinate system. Assume the flow is supersonic i.e., the system of equations is hyperbolic, then the system can be written in characteristic form:

$$\mathbf{G}_j^* \mathbf{U}_\eta + \lambda_j \mathbf{G}_j^* \mathbf{U}_\xi = f_j, \quad j = 1, \cdots, 6. \tag{12}$$

where, $\mathbf{U} = (p, h, \sigma, q_1, q_2, q_3)^*$.

3. Boundary conditions

We will formulate implicit and explicit finite difference methods. The system of equations under consideration is integrated according to the space-marching technique along the coordinate η. At a typical mesh point, all the equations are approximated by two-step second-order finite difference equations. Since we are dealing with the Euler equations and chemical equations fully coupled, there are possible numerical difficulties associated with the stiffness. To overcome these problems, we deal with the right-hand side implicitly. We have two basic finite difference schemes, one explicit and the other implicit. They will be combined according to the boundary conditions and the characteristics of the equations.

When the discontinuities are taken as internal boundaries, the solution of flow parameters in the supersonic region is reduced to the solution of initial-boundary-value problem of first order quasi-linear hyperbolic systems with several internal boundaries. In this section, we will describe

concrete expressions of the boundary conditions and internal boundary conditions that are compatible with our system of equations. That is, at each mesh point of boundary, the number of unknowns should be the same as the sum of the number of boundary conditions and that of equations provided by the difference equations.

We have a natural boundary condition at the body :

$$V_n = 0,$$

that can be written as

$$uF_z - v = 0.$$

Therefore, we can use the relation

$$V_\xi = 0$$

as the boundary condition at the body for our computations.

Since the rate of chemical reactions is finite, the shock conditions are similar to those for perfect gas flow. The quantities of flow parameters should satisfy the R-H (Rankine-Hugoniot) conditions

$$\begin{aligned} \rho_2 V_{n,2} &= \rho_1 V_{n,1}, \\ p_2 + \rho_2 V_{n,2}^2 &= p_1 + \rho_1 V_{n,1}^2, \\ h_2 + \frac{V_{n,2}^2}{2} &= h_1 + \frac{V_{n,1}^2}{2} \end{aligned} \tag{13}$$

and

$$q_{i,2} = q_{i,1} \quad i = 1, 2, 3, \tag{14}$$

where $\mathbf{n}$ is the unit normal vector to the shock and $V_n = \mathbf{V}\cdot\mathbf{n}$. A quantity with index 1 denotes a quantity in front of the shock and index 2 means behind the shock. On the main shock the enthalpy h can be expressed as

$$h = \frac{\gamma p}{(\gamma - 1)\rho}. \tag{15}$$

In our model, the molecular vibrations are assumed to be half excited [1] behind the main shock and not excited in front of the main shock. Hence, the ratio of specific heats γ changes across the shock. In front of the main shock $\gamma_1 = 7/5$ and behind the main shock $\gamma_2 = 4/3$.

The conditions (13) and (14) also hold for the reflected shock. However, the enthalpy h is given by (3) which is different from the formula (15). Since chemical reactions are frozen across the shock, $\mathcal{Z}$ and $\sum_{i=1}^{3} h_i^0 q_i$ are the same on both sides of the shock. Therefore, the third equation of (13) becomes

$$\frac{3+\mathcal{Z}}{\mathcal{Z}}\frac{p_2}{\rho_2} + \frac{V_{n,2}^2}{2} = \frac{3+\mathcal{Z}}{\mathcal{Z}}\frac{p_1}{\rho_1} + \frac{V_{n,1}^2}{2}.$$

Let $\gamma = (3+\mathcal{Z})/3$, then $(3+\mathcal{Z})/\mathcal{Z} = \gamma/(\gamma-1)$. Therefore, the formula for p_2/p_1 in this case is :

$$\frac{p_2}{p_1} = 1 + \frac{2\gamma(M_{n,1}^2 - 1)}{\gamma+1},$$

where $M_{n,1}^2 = V_{n,1}^2/(\gamma p_1/\rho_1)$. Here, the index i means the quantities in front of the shock. From the first two equations in (13) we can have

$$\frac{\rho_1}{\rho_2} = \frac{1 + \gamma M_{n,1}^2 - p_2/p_1}{\gamma M_{n,1}^2} \tag{16}$$

and

$$\mathbf{V}_2 = \mathbf{V}_1 - V_{n,1}\left(1 - \frac{\rho_1}{\rho_2}\right)\mathbf{n}. \tag{17}$$

The two relations are true for both cases since the expression of h is not used during the derivation.

4. Numerical methods

We shall use the following symbols in describing the finite difference methods for two dimensional problems.

$$\begin{aligned}
\Delta_+ \mathbf{U}_m &= \mathbf{U}_{m+1} - \mathbf{U}_m, \\
\Delta_- \mathbf{U}_m &= \mathbf{U}_m - \mathbf{U}_{m-1}, \\
\Delta \mathbf{U}_m &= \mathbf{U}_{m+\frac{1}{2}} - \mathbf{U}_{m-\frac{1}{2}}, \\
\Delta_\lambda \mathbf{U}_m &= \begin{cases} \Delta_+ \mathbf{U}_m & \text{for} \quad \lambda < 0 \\ \Delta_- \mathbf{U}_m & \text{for} \quad \lambda > 0, \end{cases} \\
\mu f_m &= \frac{1}{2}(f_{m+\frac{1}{2}} + f_{m-\frac{1}{2}}).
\end{aligned}$$

We write each equation of (12) as follows:

$$\mathbf{G}^* \frac{\partial \mathbf{U}}{\partial \eta} + \lambda \mathbf{G}^* \frac{\partial \mathbf{U}}{\partial \xi} = f, \tag{18}$$

where $\mathbf{U} = (p, h, \sigma, q_1, q_2, q_3)^*$.

At the first step, (18) is approximated by

$$\mathbf{G}_m^{*k} \mathbf{U}_m^{k+\frac{1}{2}} = \mathbf{G}_m^{*k} \mathbf{U}_m^k - \frac{1}{2} \lambda_m^k \frac{\Delta \eta}{\Delta \xi} \mathbf{G}_m^{*k} \Delta_\lambda \mathbf{U}_m^k + \frac{1}{2} \Delta \eta f_m^{k+\frac{1}{2}}. \tag{19}$$

The right-hand side of equation (18) is approximated implicitly to overcome the difficulties arising from stiffness. The implicit term is then approximated by

$$f_m^{k+\frac{1}{2}} \approx f_m^k + Df_m^k (\mathbf{U}_m^{k+\frac{1}{2}} - \mathbf{U}_m^k), \tag{20}$$

where Df is the gradient of f and our scheme becomes

$$\begin{aligned}
\mathbf{G}_m^{*k} \mathbf{U}_m^{k+\frac{1}{2}} - \frac{1}{2} \Delta \eta Df(\mathbf{U}_m^k) \mathbf{U}_m^{k+\frac{1}{2}} \\
= \mathbf{G}_m^{*k} \mathbf{U}_m^k - \frac{1}{2} \frac{\Delta \eta}{\Delta \xi} \lambda_m^k \mathbf{G}_m^{*k} \Delta_\lambda \mathbf{U}_m^k + \frac{1}{2} \Delta \eta f_m^k \\
- \frac{1}{2} \Delta \eta Df(\mathbf{U}_m^k) \mathbf{U}_m^k.
\end{aligned} \tag{21}$$

For the second step, (18) is written as

$$\mathbf{G}^* \left(\frac{\partial \mathbf{U}}{\partial \eta} \mp \frac{\Delta \xi}{\Delta \eta} \frac{\mathbf{U}}{\partial \xi} \right) + \left(\lambda \pm \frac{\Delta \xi}{\Delta \eta} \right) \mathbf{G}^* \frac{\partial \mathbf{U}}{\partial \xi} = f. \tag{22}$$

Here, if $\lambda > 0$, then the upper signs are chosen; if $\lambda < 0$, then the lower signs are chosen. Then, we approximate (22)by

$$\mu \mathbf{G}^{*k+\frac{1}{2}}_{m \pm \frac{1}{2}} \frac{\mathbf{U}^{k+1}_m - \mathbf{U}^k_m}{\Delta \eta} \mp \mu \mathbf{G}^{*k+\frac{1}{2}}_{m \pm \frac{1}{2}} \frac{\Delta \xi}{\Delta \eta} \frac{\Delta_\lambda \mathbf{U}^k_m}{\Delta \xi}$$
$$+ \left(\mu \lambda^{k+\frac{1}{2}}_{m \pm \frac{1}{2}} \pm \frac{\Delta \xi}{\Delta \eta} \right) \mu \mathbf{G}^{*k+\frac{1}{2}}_{m \pm \frac{1}{2}} \frac{\Delta_\lambda \mathbf{U}^{k+\frac{1}{2}}_m}{\Delta \xi} = \frac{1}{2} \left(f^{k+1}_m + f^k_{m \pm 1} \right)$$

which could be written again by

$$\mu \mathbf{G}^{*k+\frac{1}{2}}_{m \pm \frac{1}{2}} \mathbf{U}^{k+1}_m$$
$$= \mu \mathbf{G}^{*k+\frac{1}{2}}_{m \pm \frac{1}{2}} \mathbf{U}^k_{m \pm 1} - \left(\frac{\Delta \eta}{\Delta \xi} \mu \lambda^{k+\frac{1}{2}}_{m \pm \frac{1}{2}} \pm 1 \right) \mu \mathbf{G}^{*k+\frac{1}{2}}_{m \pm \frac{1}{2}} \Delta_\pm \mathbf{U}^{k+\frac{1}{2}}_m$$
$$- \frac{1}{2} \Delta \eta \left(f^{k+1}_m + f^k_{m \pm 1} \right). \tag{23}$$

With the approximation

$$f^{k+1}_m \approx f^k_m + D f^{k+\frac{1}{2}}_m (\mathbf{U}^{k+1}_m - \mathbf{U}^k_m), \tag{24}$$

the scheme becomes

$$\left(\mu \mathbf{G}^{*k+\frac{1}{2}}_{m \pm \frac{1}{2}} - \frac{1}{2} \Delta \eta D f(\mathbf{U}^{k+\frac{1}{2}}_m) \right) \mathbf{U}^{k+1}_m$$
$$= \mu \mathbf{G}^{*k+\frac{1}{2}}_{m \pm \frac{1}{2}} \mathbf{U}^k_{m \pm 1} - \left(\frac{\Delta \eta}{\Delta \xi} \mu \lambda^{k+\frac{1}{2}}_{m \pm \frac{1}{2}} \pm 1 \right) \mu \mathbf{G}^{*k+\frac{1}{2}}_{m \pm \frac{1}{2}} \Delta_\pm \mathbf{U}^{k+\frac{1}{2}}_m$$
$$+ \Delta \eta \mu f^k_{m \pm \frac{1}{2}} - \frac{1}{2} \Delta \eta D f(\mathbf{U}^{k+\frac{1}{2}}_m) \mathbf{U}^k_m. \tag{25}$$

The above scheme cannot be applied at the boundary points because it requires data from the points outside the computational region. At

the boundary points, we need difference equations in which only the quantities at points in the interval $0 \le \xi \le 1$ are involved.

$$(26)\quad \mu \mathbf{G}^{*k+\frac{1}{2}}_{m\mp\frac{1}{2}} \mathbf{U}^{k+1}_{m} = \mu \mathbf{G}^{*k+\frac{1}{2}}_{m\mp\frac{1}{2}} \mathbf{U}^{k}_{m\mp 1} - \left(\frac{\Delta\eta}{\Delta\xi} \mu \lambda^{k+\frac{1}{2}}_{m\mp\frac{1}{2}} \mp 1 \right) \mu \mathbf{G}^{*k+\frac{1}{2}}_{m\mp\frac{1}{2}} \Delta_{\mp} \mathbf{U}^{k+\frac{1}{2}}_{m} + \frac{1}{2} \Delta\eta \left(f^{k+1}_{m} + f^{k}_{m\mp 1} \right).$$

$$(27)\quad \left(\mu \mathbf{G}^{*k+\frac{1}{2}}_{m\mp\frac{1}{2}} - \frac{1}{2} \Delta\eta Df(\mathbf{U}^{k}_{m}) \right) \mathbf{U}^{k+1}_{m} = \mu \mathbf{G}^{*k+\frac{1}{2}}_{m\mp\frac{1}{2}} \mathbf{U}^{k}_{m\mp 1} - \left(\frac{\Delta\eta}{\Delta\xi} \mu \lambda^{k+\frac{1}{2}}_{m\mp\frac{1}{2}} \mp 1 \right) \mu \mathbf{G}^{*k+\frac{1}{2}}_{m\mp\frac{1}{2}} \Delta_{\mp} \mathbf{U}^{k+\frac{1}{2}}_{m} + \Delta\eta \mu f^{k}_{m\mp\frac{1}{2}} - \frac{1}{2} \Delta\eta Df(\mathbf{U}^{k}_{m}) \mathbf{U}^{k}_{m}.$$

We use the scheme (25) at internal points and (27) at boundary points.

To describe the implicit method, we write the system of equations in the matrix form

$$(28)\qquad \tilde{\mathbf{A}} \frac{\partial \mathbf{U}}{\partial \eta} + \tilde{\mathbf{B}} \frac{\partial \mathbf{U}}{\partial \xi} = \mathbf{f},$$

where $\tilde{\mathbf{A}}$, $\tilde{\mathbf{B}}$ are 6×6 matrices and $\mathbf{U} = (p, h, \sigma, q_1, q_2, q_3)^*$. We consider each equation of (28) in the form

$$(29)\qquad \mathbf{A}^* \frac{\partial \mathbf{U}}{\partial \eta} + \mathbf{B}^* \frac{\partial \mathbf{U}}{\partial \xi} = f.$$

We will discretize this as follows. At the first step, consider

$$(30)\quad \mu \mathbf{A}^{*k}_{m+\frac{1}{2}} \mu \mathbf{U}^{k+\frac{1}{2}}_{m+\frac{1}{2}} + \frac{1}{2} \frac{\Delta\eta}{\Delta\xi} \mu \mathbf{B}^{*k}_{m+\frac{1}{2}} \Delta \mathbf{U}^{k+\frac{1}{2}}_{m+\frac{1}{2}} = \mu \mathbf{A}^{*k}_{m+\frac{1}{2}} \mu \mathbf{U}^{k}_{m+\frac{1}{2}} + \frac{1}{2} \Delta\eta \mu f^{k+\frac{1}{2}}_{m+\frac{1}{2}}$$

and then use the approximation (20) at $m + \frac{1}{2}$ to obtain

$$(31)\quad \mu\mathbf{A}^{*k}_{m+\frac{1}{2}}\mu\mathbf{U}^{k+\frac{1}{2}}_{m+\frac{1}{2}} + \frac{1}{2}\frac{\Delta\eta}{\Delta\xi}\mu\mathbf{B}^{*k}_{m+\frac{1}{2}}\Delta\mathbf{U}^{k+\frac{1}{2}}_{m+\frac{1}{2}} - \frac{1}{2}\Delta\eta\mu\left[Df^{k}_{m+\frac{1}{2}}\mathbf{U}^{k+\frac{1}{2}}_{m+\frac{1}{2}}\right] = \mu\mathbf{A}^{*k}_{m+\frac{1}{2}}\mu\mathbf{U}^{k}_{m+\frac{1}{2}} + \frac{1}{2}\Delta\eta\mu f^{k}_{m+\frac{1}{2}} - \frac{1}{2}\Delta\eta\mu\left[Df^{k}_{m+\frac{1}{2}}\mathbf{U}^{k}_{m+\frac{1}{2}}\right]$$

or when grouped in m,

$$(32)\quad \frac{1}{2}\left(\mu\mathbf{A}^{*k}_{m+\frac{1}{2}} + \frac{\Delta\eta}{\Delta\xi}\mu\mathbf{B}^{*k}_{m+\frac{1}{2}} - \frac{1}{2}\Delta\eta Df^{k}_{m+1}\right)\mathbf{U}^{k+\frac{1}{2}}_{m+1} + \frac{1}{2}\left(\mu\mathbf{A}^{*k}_{m+\frac{1}{2}} - \frac{\Delta\eta}{\Delta\xi}\mu\mathbf{B}^{*k}_{m+\frac{1}{2}} - \frac{1}{2}\Delta\eta Df^{k}_{m}\right)\mathbf{U}^{k+\frac{1}{2}}_{m} = \mu\mathbf{A}^{*k}_{m+\frac{1}{2}}\mu\mathbf{U}^{k}_{m+\frac{1}{2}} + \frac{1}{2}\Delta\eta\mu f^{k}_{m+\frac{1}{2}} - \frac{1}{2}\Delta\eta\mu\left[Df^{k}_{m+\frac{1}{2}}\mathbf{U}^{k}_{m+\frac{1}{2}}\right]$$

For the second step, consider

$$(33)\quad \mu\mathbf{A}^{*k+\frac{1}{2}}_{m+\frac{1}{2}}\mu\mathbf{U}^{k+1}_{m+\frac{1}{2}} + \frac{1}{2}\frac{\Delta\eta}{\Delta\xi}\mu\mathbf{B}^{*k+\frac{1}{2}}_{m+\frac{1}{2}}\Delta\mathbf{U}^{k+1}_{m+\frac{1}{2}} = \mu\mathbf{A}^{*k+\frac{1}{2}}_{m+\frac{1}{2}}\mu\mathbf{U}^{k}_{m+\frac{1}{2}} - \frac{1}{2}\frac{\Delta\eta}{\Delta\xi}\mu\mathbf{B}^{*k+\frac{1}{2}}_{m+\frac{1}{2}}\Delta\mathbf{U}^{k}_{m+\frac{1}{2}} + \frac{1}{2}\Delta\eta\left[\mu f^{k}_{m+\frac{1}{2}} + \mu f^{k+1}_{m+\frac{1}{2}}\right]$$

then use the approximation (24) at $m + \frac{1}{2}$ to obtain our scheme

$$(34)\quad \mu\mathbf{A}^{*k+\frac{1}{2}}_{m+\frac{1}{2}}\mu\mathbf{U}^{k+1}_{m+\frac{1}{2}} + \frac{1}{2}\frac{\Delta\eta}{\Delta\xi}\mu\mathbf{B}^{*k+\frac{1}{2}}_{m+\frac{1}{2}}\Delta\mathbf{U}^{k+1}_{m+\frac{1}{2}} - \frac{1}{2}\Delta\eta\mu\left[Df^{k+\frac{1}{2}}_{m+\frac{1}{2}}\mathbf{U}^{k+1}_{m+\frac{1}{2}}\right] = \mu\mathbf{A}^{*k+\frac{1}{2}}_{m+\frac{1}{2}}\mu\mathbf{U}^{k}_{m+\frac{1}{2}} - \frac{1}{2}\frac{\Delta\eta}{\Delta\xi}\mu\mathbf{B}^{*k+\frac{1}{2}}_{m+\frac{1}{2}}\Delta\mathbf{U}^{k}_{m+\frac{1}{2}} + \Delta\eta\mu f^{k}_{m+\frac{1}{2}} - \frac{1}{2}\Delta\eta\mu\left[Df^{k+\frac{1}{2}}_{m+\frac{1}{2}}\mathbf{U}^{k}_{m+\frac{1}{2}}\right]$$

or when grouped in m the scheme becomes,

$$
\begin{aligned}
(35)\quad & \frac{1}{2}\left(\mu \mathbf{A}^{*k+\frac{1}{2}}_{m+\frac{1}{2}} + \frac{\Delta\eta}{\Delta\xi}\mu \mathbf{B}^{*k+\frac{1}{2}}_{m+\frac{1}{2}} - \frac{1}{2}\Delta\eta D f^{k+\frac{1}{2}}_{m+1}\right)\mathbf{U}^{k+1}_{m+1} \\
& + \frac{1}{2}\left(\mu \mathbf{A}^{*k+\frac{1}{2}}_{m+\frac{1}{2}} - \frac{\Delta\eta}{\Delta\xi}\mu \mathbf{B}^{*k+\frac{1}{2}}_{m+\frac{1}{2}} - \frac{1}{2}\Delta\eta D f^{k+\frac{1}{2}}_{m}\right)\mathbf{U}^{k+1}_{m} \\
& = \mu \mathbf{A}^{*k+\frac{1}{2}}_{m+\frac{1}{2}}\mu \mathbf{U}^{k}_{m+\frac{1}{2}} - \frac{1}{2}\frac{\Delta\eta}{\Delta\xi}\mu \mathbf{B}^{*k+\frac{1}{2}}_{m+\frac{1}{2}}\Delta \mathbf{U}^{k}_{m+\frac{1}{2}} \\
& \qquad + \Delta\eta\mu f^{k}_{m+\frac{1}{2}} - \frac{1}{2}\Delta\eta\mu\left[D f^{k+\frac{1}{2}}_{m+\frac{1}{2}}\mathbf{U}^{k}_{m+\frac{1}{2}}\right].
\end{aligned}
$$

5. Numerical results

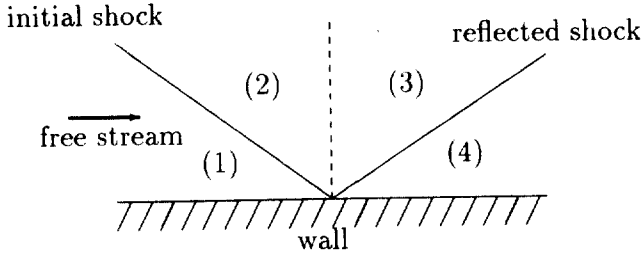

Figure 1: Flow Patterns at the Reflection Point

Figure 1 shows a qualitative picture of the flow in a neighborhood of shock reflection point. The initial flow in (1) is free stream that is uniform and parallel to the body. The flow in (2), behind the main shock, is nonequilibrium flow. The reflected shock is formed when the main shock hits the wall. The flow in (3) behind the reflected shock has much higher temperature and pressure than the flow in (2). Therefore, chemical reaction is very strong behind the reflected shock and the computation of the flow is difficult because of the stronger stiffness and higher gradient of functions than the flow in (2). The location of the reflected shock can be determined by the jump conditions at the reflected shock.

We have done some numerical experiments with free stream conditions as in Table 1.

Table 1. Free Stream Conditions

Speed	$6.77 Km/s$
Altitude	$65 Km$
Pressure	$10.85 N/m^2$
Density	$1.56 \times 10^{-4} Kg/m^3$
Mach Number	21.7

The system of equations under consideration is integrated according to the space-marching technique along the coordinate η. We treat the shock with shock-fitting technique. The R-H conditions give the jump conditions. If the slope of the shock is known, the quantities behind the shock can be determined by the R-H conditions. In practice, we guess the slope of the shock and use an iteration method to match the computed quantities with the equation obtained from finite difference method.

Our computation starts at a concave corner of the body to generate the initial shock. The body has a 25 degree concave corner against the free stream. The shock was reflected at $25.7\,m$ down stream from the corner. We have chosen a relatively long distance because the computation becomes more difficult as we go down stream. Since we have reported the complete analysis of the flow behind the main shock in [3], we will analyze the flow behind the reflected shock by presenting the result in that region only. We present concentration of NO and temperature in Figures 2 and 3.At the reflection point, the concentrations of species O, N and NO are 0 because the chemical reactions are just beginning to occur at that point. The temperature at the reflection point in region (3) is $9435\,K$. $z = 0\,m$ at the reflection point and the results are reported at $z = .003\,m$ (dashed line), $z = .252\,m$ (dotted line), $z = 2.18\,m$ (dash-and-dot), and $z = 6.18\,m$ (solid line). The concentration of NO is in unit $g\text{-}mole/g$ and the temperature is in K.

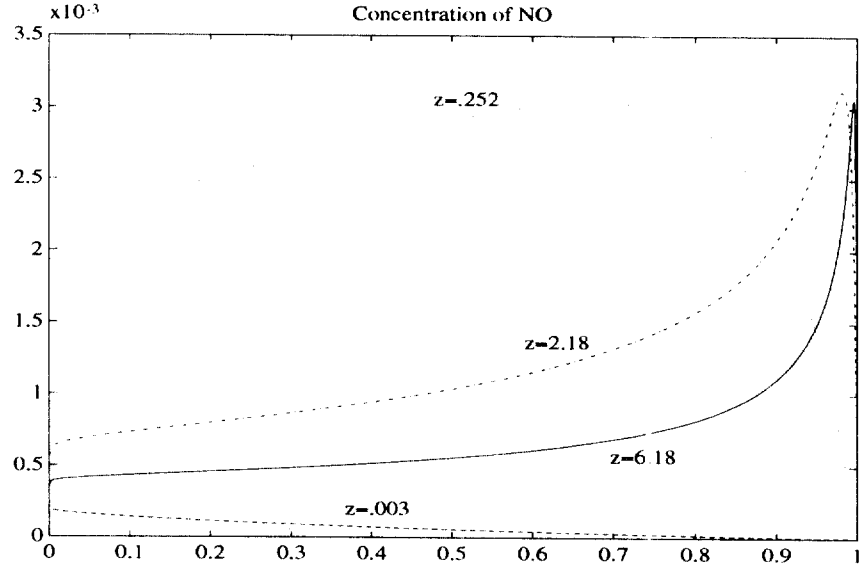

Figure 2: Concentration of NO after shock reflection (g-mole/g)

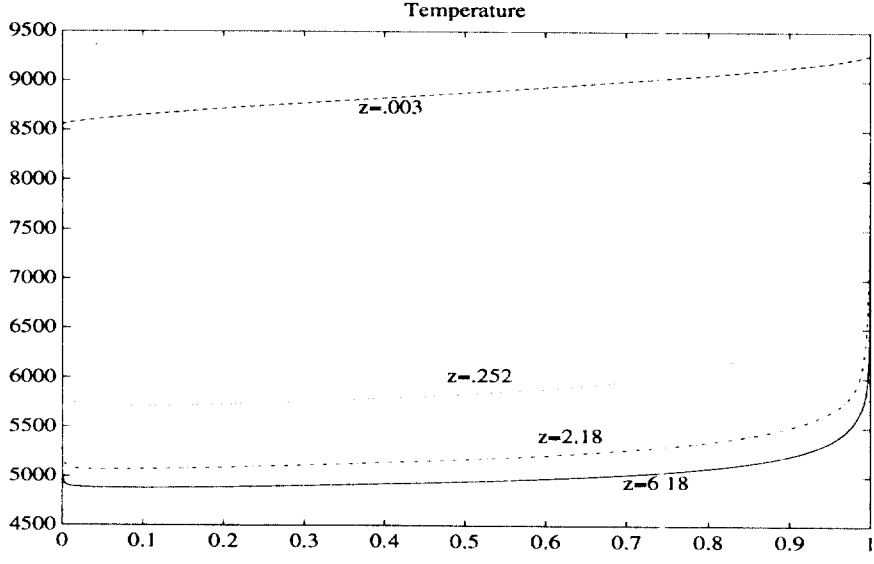

Figure 3: Temperature after shock reflection (K)

References

1. Lighthill, M. L., *Dynamics of Dissociating Gas, Part I: Equilibrium Flow*, Journal of Fluid Mechanics **2** (1957), 1-32..
2. Pandolfi, M., Arina, R. and Botta, N., *Nonequilibrium Hypersonic Flows over Corners*, AIAA Journal **29** (1991), 235-241..
3. Park, T., *Computation of Nonequilibrium Hypersonic Inviscid Flow over Concave Corners*, Computers & Fluids (to appear).
4. Park, T., *Second Shock in Nonequilibrium Hypersonic Inviscid Flow*, preprint.
5. Rakich, J. V., Bailey, H. E. and Park, C., *Computation of Nonequilibrium, Supersonic Three-Dimensional Inviscid flow over Blunt-Nosed Bodies*, AIAA Journal **21** (1983), 834-841.
6. Vincenti, W. G. and Kruger, C. M., *Introduction to Physical Gas Dynamics*, Wiley, New York, 1965.
7. Zhu, Y.-l., Zhong, X.-c., Chen, B.-m. and Zhang, Z.-m., *Difference Methods for Initial-Boundary-Value Problems and Flow Around Bodies*, Springer-Ver- lag, Heidelberg and Science Press, Beijing, 1988.

Topology and Geometry Research Center
Kyungpook National University
Taegu 702-701, KOREA